Accurate analysis of Mg2+ binding to RNA: From classical methods to a novel iterative calculation procedure

Erat, M C ; Coles, J ; Finazzo, C ; Knobloch, B ; Sigel, Roland K O

Abstract: Mg2+ acts as a catalytic cofactor in many ribozymes and specifically bound divalent metal ions have been implicated in the stabilization of structural motifs that are essential for RNA folding. The accurate calculation of intrinsic affinity constants of M2+ to specific binding sites in nucleic acids is therefore of high importance. Methods classically applied to determine the affinity constants of metal ions to RNAs are summarized in the first part of this review, e.g. hydrolytic cleavage experiments, equilibrium dialysis, and spectroscopic techniques like EPR and NMR. However, the fact that several binding sites of similar affinities are often present in a single RNA molecule is mostly neglected. The most immediate consequence of several binding sites is that less than the total amount of M2+ is available to bind to a particular binding site at a given total concentration. We have recently introduced a new iterative procedure that tackles this problem and have developed a rapid calculation tool (ISTAR) that is available from the authors. Here, we explain this procedure in detail under different assumptions and illustrate how the intrinsic affinity constants for Mg2+ to a short RNA hairpin, a minimal domain 6 from the group II intron Sc.ai5 gamma, change. We use ISTAR to calculate intrinsic affinities and to validate a particular binding stoichiometry by judging the quality of the fit to the experimental data for a given model. This is important since weak coordination sites exhibiting similar binding affinities, and being thus in direct competition to each other, are a characteristic feature of nucleic acids. With ISTAR these binding affinities can be calculated more accurately within minutes and we can gain a better understanding of these crucial metal ion-nucleic acid interactions.

DOI: https://doi.org/10.1016/j.ccr.2011.08.009

How to analyze accurately Mg^{2+} binding to RNA. From classical methods to a novel iterative calculation procedure

Michèle C. Erat[a,b], Jonathan Coles[c], Cinzia Finazzo[a], Bernd Knobloch[a]

and Roland K. O. Sigel[a]*

[a] *Institute of Inorganic Chemistry, University of Zürich,Winterthurerstrasse 190, CH-8057 Zürich, Switzerland*

[b] *Department of Biochemistry, University of Oxford, South Parks Road, Oxford OX1 3QU, UK*

[c] *Institute of Theoretical Physics, University of Zürich, Winterthurerstrasse 190, CH-8057 Zürich, Switzerland*

Corresponding author. Tel: +41-44-635 4652; Fax: +41-44-635 6802
E-mail address: roland.sigel@aci.uzh.ch

Contents

Abstract

1. Introduction
2. Group II intron domains as metal ion binding platforms
3. Classical determination of metal ion affinity constants to RNA
    3.1. Hydrolytic cleavage experiments
    3.2. Competition and equilibrium dialysis experiments
    3.3. X-ray, EPR, and NMR spectroscopy
4. Calculation of intrinsic affinity constants for Mg^{2+} binding to several sites in a single RNA
    4.1. Experimental techniques used to define individual binding sites
    4.2. Domain 6, a distinct metal ion binding platform
        4.2.1. Determination of the number of binding sites and calculation of initial affinity constants
        4.2.2. Calculation of intrinsic affinity constants
        4.2.3. ISTAR – A tool for calculating the *I*ntrinsic *STA*bilities of RNA complexes
        4.2.4. Determination of the binding stoichiometry by ISTAR
5. Conclusions and outlook

Abbreviations and definitions

Acknowledgements

References

Abstract

Mg^{2+} acts as a catalytic cofactor in many ribozymes and specifically bound divalent metal ions have been implicated in the stabilization of structural motifs that are essential for RNA folding. The accurate calculation of intrinsic affinity constants of M^{2+} to specific binding sites in nucleic acids is therefore of high importance. Methods classically applied to determine the affinity constants of metal ions to RNAs are summarized in the first part of this review, e.g. hydrolytic cleavage experiments, equilibrium dialysis, and spectroscopic techniques like EPR and NMR. However, the fact that several binding sites of similar affinities are often present in a single RNA molecule is mostly neglected. The most immediate consequence of several binding sites is that less than the total amount of M^{2+} is available to bind to a particular binding site at a given total concentration. We have recently introduced a new iterative procedure that tackles this problem and have developed a rapid calculation tool (ISTAR) that is available from the authors. Here, we explain this procedure in detail under different assumptions and illustrate how the intrinsic affinity constants for Mg^{2+} to a short RNA hairpin, a minimal domain 6 from the group II intron Sc.ai5γ, change. We use ISTAR to calculate intrinsic affinities and to validate a particular binding stoichiometry by judging the quality of the fit to the experimental data for a given model. This is important in the light that weak coordination sites exhibiting similar binding affinities and being thus in direct competition to each other, are a characteristic feature of nucleic acids. With ISTAR these binding affinities can be calculated more accurately within minutes and thus a better understanding of these crucial metal ion-nucleic acid interactions is gained.

Keywords: Group II intron, RNA, affinity constants, metal ion binding, NMR, ISTAR

1. Introduction

All large ribozymes, i.e. catalytic RNA molecules, are compulsory "metalloenzymes", using metal ions to fold into their active three dimensional structure, to enhance the reactivity of the involved species, and/or to stabilize the transition state [1-3]. Compared to proteins, RNA has a rather low affinity for metal ions (usually with K_D values in the order of 10^{-3} M), a fact that has been attributed to the high flexibility of the nucleic acid backbone and the less dense packing in RNA structures [4,5]. Thus RNA active sites are probably more dynamic and involve a network of stacking and hydrogen bonding interactions. Specifically located, but relatively weakly bound metal ions play a crucial role for the stability of these complex structures.

Potential binding sites include atoms that are deprotonated at physiological pH, such as the nonbridging oxygens of the phosphodiester linkage, the N7 and N3 nitrogens in purines [6], the N1 moiety in adenine [7], N3 in cytosine, as well as the carbonyl groups in guanosine and the pyrimidines (Fig. 1) [4,8,9]. Depending on which M^{2+} ion is used *in vivo* and *in vitro* experiments, one or the other liganding atom will become more important [8,10]. One can assume that the negatively charged phosphate oxygens are the most prominent primary binding site. In the case of Hammerhead riboyzmes, the catalytic activity can be directly linked to the respective affinity of the M^{2+} to a phosphate group [11-14]. On the other hand, no such obvious correlation exists for another small catalytic RNA, the *glmS* ribozyme [15]. Nevertheless, it is clear that the kind of metal ions, and thus their coordination properties determine the catalytic activity to a large part.

Figure 1 close to here

With a given kind of labile metal cation, binding sites in an RNA molecule can be classified into two groups according to their affinities: Whereas a few high affinity binding sites are important for the initial structural arrangement [16-18], the fine-tuning of an active site may require the population of specific low affinity binding sites [16,19]. Thus coordination sites with dissociation constants in the millimolar range are most likely of fundamental importance for

ribozyme chemistry. Finding reliable tools for the characterization of such low affinity binding sites is therefore of high relevance for the elucidation of the detailed mechanisms by which catalytic RNAs operate. Classically, such affinity constants have been determined by assuming a simple 1:1 equilibrium scheme and evaluating spectroscopic data from various sources, e.g. NMR, fluorescence, and UV/Vis, but also gel electrophoresis studies. All these studies assume that at each titration step, the total added metal ion concentration is available to each binding site at any given moment. We have recently demonstrated that this assumption clearly does not hold for some systems: The individual binding sites compete for the metal ions, which has a profound influence on the available metal ion concentration unless a large excess of metal ions is present [20].

We now first introduce the group II intron ribozyme Sc.ai5γ and its domains as a perfect system to investigate metal ion binding to RNA as well as these ions' influence on structure and catalysis. Second, the different methods generally applied in the past that are based on a 1:1 binding equilibrium scheme are summarized. In the following, we describe the recently introduced iterative calculation procedure for the calculation of accurate intrinsic metal ion affinity constants derived from chemical shift change analyses by NMR [20]. By taking into account the reduced metal ion concentration available to each binding site at any given time-point due to simultaneous occupation of other sites, a significantly better fit of the experimental data is achieved. Finally, having automated this calculation procedure, we discuss if such calculations of intrinsic binding constants can be used to determine or validate binding stoichiometries for weak metal ion-nucleic acid interactions.

2. Group II intron domains as metal ion binding platforms

Group II introns are naturally occurring, highly structured self-splicing ribozymes that consist of six domains, each with a distinct functionality [21,22]. As for all large ribozymes, metal ions play a crucial role for their folding and catalysis [3,4,13,23]. The yeast mitochondrial group II

intron *Sc*.ai5γ is one of the best-characterized large ribozymes. Folding of *Sc*.ai5γ is devoid of kinetic traps and proceeds via two on pathway intermediates under near-physiological conditions *in vitro* [24-26]. This process depends critically on the presence of Mg^{2+}, however, even low levels of Ca^{2+} competitively inhibit *in vitro* splicing [27] by locking a subpopulation of ribozymes in an inactive state [28]. D5, the catalytic domain and D6, which harbors the nucleophile for the first splicing step, are hairpins of only ~35 nucleotides in length and thus not only suited for structural analysis by NMR spectroscopy (Fig. 2), but are also typical representatives for RNA molecules in general. The corresponding structures have recently been published [29,30].

Figure 2 close to here

The metal ion binding properties of D5 and D6 of *Sc*.ai5γ have been analyzed in detail in the past [20,29,31]. Within both hairpins four to five specific internal binding sites have been identified and described [20,31,32]. Thus D5 and D6 act as specific binding platforms for divalent Mg^{2+} ions (Fig. 2), providing the necessary charge compensation for docking of these two domains into the active site of the ribozyme. Furthermore, divalent metal ions are likely to act as cofactors in the splicing mechanism of large ribozymes by increasing the nucleophilicity of the attacking 2'-OH and by stabilizing the pentavalent transition state and the negatively charged leaving group [33,34]. Indeed, two metal ions were located in the bulge and the catalytic triad of D5 in the crystal structure of a group II intron from *Oceanobacillus iheyensis* [35,36]. The docking of D5 and D6 seems to be at the end of the folding pathway and is possibly directly followed by splice site formation and subsequent splicing. However, in order to understand this last docking step, detailed knowledge of the metal ion binding on the individual domains D5 and D6 is necessary.

3. Classical determination of metal ion affinity constants

3.1. Hydrolytic cleavage experiments

Hydrolytic cleavage has been commonly used to probe metal ion binding to RNA. A variety of different approaches was recently reviewed in detail [14]. Water molecules in the inner solvation shell of metal ions can either attack the phosphodiester bond of the RNA directly or can activate the ribose 2'-OH upon partial deprotonation. Cleavage sites can be located by gel electrophoresis and directly indicate metal ion binding sites.

Probably the first metal ion to be applied in this respect was Pb^{2+}. Already in the 1980s metal ion binding sites in tRNA have been identified by Pb^{2+} induced cleavage [37,38]. But with the notable exception of the leadzyme [39,40], Pb^{2+} induced cleavage is usually relatively weak and unspecific [31,41]. Nevertheless, due to its preferred attack on single stranded regions, it has been used extensively as a probe for stable secondary structure elements in RNAs [42,43] and to follow conformational changes upon folding or catalysis [44].

More common probes to identify metal ion binding sites are lanthanide(III) ions (Ln^{3+}), which are used as Mg^{2+} mimics. Although they are slightly larger than Mg^{2+} they have been shown to bind to the same or similar locations in RNA [45]. Like Mg^{2+} they prefer hard ligands, such as the phosphate oxygen of the RNA backbone, and are (mostly) not very redox active. Due to their +3 charge, they have a high affinity for the polyanionic RNA backbone. Ln^{3+} ions accelerate hydrolysis of a phosphodiester bond near the site of binding because the water molecules coordinated to the Ln^{3+} ion exhibit a pK_a close to neutral pH [14]. Lanthanide(III) induced cleavage has been used to define Mg^{2+} ion binding sites in a variety of ribozymes, such as the hairpin and the hepatitis delta virus ribozymes [46,47], a group II intron ribozyme [31] and even the ribosome [48]. Folded tertiary structures are usually not disrupted upon addition of Ln^{3+}. On the other hand, Ln^{3+} ions are able to interfere with folding when added prematurely [46]. In a study with the *Sc*.ai5γ group II intron from yeast, testing a wide concentration range of Tb^{3+} and Lu^{3+} [31], the two different Ln^{3+} ions showed identical binding loci and cleavage intensities. Whereas millimolar concentrations lead to indiscriminate cleavage of poorly structured regions, lower concentrations could trace a variety of metal ion binding sites with

different affinities, from 250 ± 50 μM to 63 ± 15 mM [31,45]. As a large excess of Ln^{3+} is used in such studies (>1000 fold), independent 1:1 binding stochiometries for each binding site always taking the total Ln^{3+} concentration into account can be assumed. It was also demonstrated that all major observed Ln^{3+} binding sites were bona-fide coordination sites for Mg^{2+} ions, as Mg^{2+} was able to compete for Ln^{3+} binding. Further evidence for the relevance of Ln^{3+} as a Mg^{2+} mimic, was the fact that at elevated pH, Mg^{2+} itself leads to cleavage at identical sites in the RNA [31]. Thus, Ln^{3+} induced cleavage is a sensitive method to trace metal ion binding sites in RNA across a wide range of affinities. One advantage of the method is the fact that it can also be applied to very large RNAs, as long as unspecific degradation can be limited.

Unfortunately, not all metal ion binding sites are detected by this method because cleavage of the RNA backbone by a scissile 2'-hydroxyl highly depends on the local geometry [37,45]. Even strong metal ion binding sites can therefore go undetected if they are located within helical regions of the RNA. Furthermore, this technique is very sensitive to changes in experimental conditions (pH, salt concentration, cleavage temperature), which have to be optimized for every new RNA under investigation. This renders the method relatively time consuming and care has to be taken to include adequate control experiments to account for spontaneous RNA degradation over time.

3.2. Competition and equilibrium dialysis experiments

Hydrolytic cleavage experiments can be used indirectly to calculate affinities for Mg^{2+} binding sites in folded RNA: The Ln^{3+} affinity at each cleavage site is calculated by plotting the in band intensity against Ln^{3+} concentration. This experiment is repeated at different Mg^{2+} concentrations. From the dependence of the Ln^{3+} affinities on the Mg^{2+} concentration, the affinity of Mg^{2+} at a specific binding pocket can be calculated [14]. Unfortunately, although this method is fairly time consuming and it is not possible to define binding sites very accurately. On the other hand, it is probably the only method that does not have an inherent size limit and hence

even very large RNAs can be examined.

To measure the total amount of Mg^{2+} bound to an RNA, the best method described in the literature is "forced equilibrium dialysis" [49]. An equilibrated RNA-metal ion mixture is loaded on a centricon ultrafiltration device. A small part of the solution is allowed to pass though the membrane and the metal ion content of the separated samples is analyzed by either atomic absorption spectroscopy or fluorescence spectroscopy. A drawback to this method is that it does not provide any information on the sites of coordination.

3.3. X-ray, EPR, and NMR spectroscopy

The most direct method to visualize metal ion coordination to RNA is to solve high resolution crystal structures. With sufficient resolution, alkaline and alkaline earth metal ions can be directly observed, as exemplified in the structure of the large ribosomal subunit of *Haloarcula marismortui*, where 116 Mg^{2+} and 88 monovalent metal ions have been identified [50]. A difficulty with this approach is the fact that Na^{+}, Mg^{2+} and H_2O are only (if at all) distinguishable at very high resolution due to their equal number of electrons [51]. More often than not, one has to use heavier metal soaking to identify metal ion binding sites in macromolecular crystals [52]. As no two metals will bind in exactly the same fashion due to their different size, charge and ligand binding properties, any discovered metal ion binding site will have to be confirmed with relevant biochemical or alternative spectroscopic methods. In any case, X-ray structures alone will not yield any thermodynamic information on metal ion binding.

Another technique often used in this context is Electron Paramagnetic Resonance spectroscopy (EPR): The paramagnetic Mn^{2+} ion can be used as a Mg^{2+}-mimic to directly detect metal ion binding. Although Mn^{2+} is slightly larger than Mg^{2+} and exchanges faster with the solvent at an RNA binding site, it shows generally similar binding properties, such as an octahedral coordination and preferred binding to relatively hard ligands such as oxygen [10,13,14]. Recently developed methods have enabled researchers to identify the ligating atoms

and measure distant restraints to characterize a specific metal ion binding site [53]. In addition, competition experiments with Cd^{2+} have yielded estimates of binding affinities as well as a number of metal ion binding sites and the order in which they are filled [54].

The focus of this review however, lies on the use of Nuclear Magnetic Resonance (NMR) for the determination of metal ion binding sites in RNA. The chemical shift of an NMR active nucleus is highly sensitive to changes in its electronic environment, e.g. induced upon conformational changes or metal ion interaction. These chemical shift changes can then be plotted against the metal ion concentration of a titration series and fitted to a 1:1 bimolecular association curve to calculate affinity constants [29,30]. An advantage of the method is that Mg^{2+}, the most common divalent metal ion to bind nucleic acids *in vivo*, does not have to be replaced by a mimic.

A simple measure of whether Mg^{2+} has any influence on a particular RNA is to observe the ^{1}H chemical shift of uracil NH3 and guanine NH1 upon metal ion addition [29,55]. These imino protons, however, are distant from potential metal ion binding sites such as the phosphate backbone, the N7 of purines, the carbonyl oxygens of guanosine, cytosine and uracil or the 2'-OH of the ribose. Furthermore, adenosines and cytosines that do not have an imino group are not observable at all. At higher temperatures and when not involved in hydrogen bonding, imino protons often show broadened linewidths due to increased solvent exchange which makes them difficult to observe [29]. Hence it is advisable to turn to more sophisticated NMR experiments for reliable detection and quantification of metal ion binding sites in nucleic acids.

Several attempts have been made to examine metal ion coordination through direct ^{31}P [56] or ^{15}N [57,58] detection. However, insufficient resolution in the case of phosphorus and the low signal intensity due to the low gyromagnetic ratio of ^{15}N make it very difficult to obtain exact information in a reasonable timeframe. Thus most people rely on proton based experiments, such as the two-dimensional ^{1}J-[$^{1}H^{13}C$]-HSQC [59] or [$^{1}H^{1}H$]-NOESY experiments [20,29,30]. Recently, also ^{2}J-[$^{1}H^{15}N$]-HSQCs have been implemented to directly follow the chemical shift

changes of the purine N7 and H8 upon metal ion titration [32,60].

4. Calculation of intrinsic affinity constants for Mg^{2+} binding to several sites in a single RNA

4.1. Experimental techniques used to define individual binding sites

In order to determine intrinsic affinity constants, the experimental technique has to meet one important requirement: The observable needs to be affected by only a single metal ion. In other words, it must not correspond to the averaged effect of two or more binding sites. Two-dimensional NMR spectra allow observation of ^{1}H, ^{13}C, ^{15}N, or ^{31}P chemical shift changes of individual atoms and in many cases also of individual binding sites. To calculate exact intrinsic affinity constants, it is important to collect data from as many nuclei as possible. A good experiment in this respect is the classic [$^{1}H^{1}H$]-NOESY, which reports on the non-exchangeable protons H8, H2, H6, H5 and H1' that are relatively close to potential metal ion binding sites (see Section 1 and Fig. 11).

Because chemical shift deviations can also indicate conformational changes, additional confirmation for metal ion binding is desirable. To this end, line-broadening analyses by titration with paramagnetic Mn^{2+} have been employed [10,20,59,61]. The single unpaired electron in Mn^{2+} causes a rapid relaxation of nuclear spins in its vicinity with an r^{-6} distance dependence [62]. Line-broadening studies performed with micromolar amounts of Mn^{2+} can therefore pin-point protons in close contact to the metal ion. But binding of the diamagnetic Mg^{2+} ion also often leads to a certain degree of linewidth broadening, due to an intermediate exchange regime of the ions at their binding site on the NMR timescale (μs-ms) [14]. This additional piece of information helps to define which of the chemical shift changes arise from Mg^{2+} binding in close proximity and which are induced over larger distances.

4.2. Domain 6, a distinct metal ion binding platform

4.2.1. Determination of the number of binding sites and calculation of initial affinity constants

The minimal branch-domain 6 of *Sc*.ai5γ (D6-27), whose solution structure we have solved to an r.m.s.d. for all heavy atoms of 1.18 ± 0.37 Å (Fig. 2B) [30], represents an ideal object to study metal ion binding. Its NMR spectra are relatively well resolved and the tetraloop as well as the two GU wobble pairs that flank the single nucleotide bulge of the branch-point represent two characteristic metal ion binding sites of RNA. In total, D6-27 has up to five distinct metal ion binding sites [20] and actively supports trans-branching *in vitro* [30]. The obtained results are thus relevant in a biological context.

To elucidate the four internal metal ion binding sites mentioned above and the strong coordination site at the triphosphate 5'-end of this *in vitro* transcribed RNA (Fig. 2B), we performed extensive NMR titration experiments with Mg^{2+}, Mn^{2+}, Cd^{2+} and $[Co(NH_3)_6]^{3+}$ [20,30,32]. The ^1H chemical shift changes induced by Mg^{2+} were used to calculate the affinity constant of the metal to a specific binding site in RNA by plotting the chemical shift change in ppm versus the added $[Mg^{2+}]$ and subsequently fitting these curves to a Levenberg-Marquart nonlinear least-squares regression for a 1:1 bimolecular association scheme [20,29,61,63].

For reasons described in Section 4.1, we monitored the chemical shift change for the H8, H2, H6, H5 and H1' protons by 2D [$^1H^1H$]-NOESY spectra. Out of 71 evaluated protons, 41 could be reasonably well fit to a 1:1 binding isotherm, yielding dissociation constants K_D in the low millimolar range for each of these protons [20]. Even though these values seem to be more or less equal for all protons at first sight, a closer examination revealed a clustering within the error limits of the affinity constants at distinct sites within D6-27 (Fig. 2B).

To define the protons that were part of an individual binding site, we took advantage of the line-broadening effect that Mg^{2+}-coordination has on RNA due to its exchange rate which comes close to the intermediate exchange limit on the NMR timescale (see also above) [30]. We also used Mn^{2+} as a probe to distinguish between chemical shift effects derived from direct metal ion binding versus conformational changes within the RNA [20].

Initially five binding sites were defined for D6-27 (Fig. 2B) [20]: The 5'-terminal phosphate groups (triphosphate, TP; diphosphate, DP), the tandem GC pairs in helix 1 (H1), the branch region (BR), the tetraloop (TL), as well as the basepairs right below in helix 2 (H2). For each binding site "i" the equilibrium

$$RNA_i + Mg^{2+} \rightleftharpoons RNA_i \bullet Mg^{2+} \qquad (1a)$$

and the corresponding definition of its affinity constant

$$K_{Ai} = \frac{\left[RNA_i \bullet Mg^{2+}\right]}{\left[Mg^{2+}\right]\left[RNA_i\right]} \qquad (1b)$$

holds. The total concentration of Mg^{2+} is defined by

$$\left[Mg^{2+}\right]_{tot} = \left[RNA_i \bullet Mg^{2+}\right]_i + \left[Mg^{2+}\right]_{tot-i} \qquad (2)$$

and the total concentration of each binding site i by

$$\left[RNA_i\right]_{tot} = \left[RNA_i \bullet Mg^{2+}\right]_i + \left[RNA\right]_{tot-i} \qquad (3).$$

$[RNA \cdot Mg^{2+}]_i$ is the amount of the complexed binding site i, whereas $[Mg^{2+}]_{tot-i}$ and $[RNA]_{tot-i}$ correspond to the concentrations of the free species in solution (see also [20]).

The log K_A values obtained from the fit of the chemical shift changes of the protons belonging to a given binding site were averaged to obtain one affinity constant for each site (Table 1A). At the 5'-end, we calculated one value for the triphosphate that was present in about one third of the molecules ($\log K_{A,av1,TP} = 3.15 \pm 0.11$) and a second one for the diphosphate whose chemical shift represented about two thirds of the RNA ($\log K_{A,av1,DP} = 2.35 \pm 0.04$).

Table 1 close to here

The above affinity constants were calculated based on the assumption that in each titration step the full Mg^{2+} concentration is available for coordination at every binding site. However, the relatively narrow range of the determined dissociation constants shows that all internal binding sites fill up simultaneously. An exception is the terminal 5'-triphosphate, which shows a 15-fold

higher affinity for Mg^{2+} than all the other binding sites (the diphosphate groups shows a 4 fold increase in affinity) [20]. Thus, the assumption that the whole Mg^{2+} concentration is available at each binding sites at all times cannot hold. So far, RNA-metal ion binding studies performed by NMR have to a large degree neglected this fact [29,63,64].

4.2.2. Calculation of intrinsic affinity constants

To take into account that not all of the Mg^{2+} titrated to the solution is actually available at every binding site, we have developed an iterative calculation procedure [20]. First the amount of bound Mg^{2+} at one specific binding site (i) is determined according to *equation 4*:

$[RNA{\cdot}Mg^{2+}]_i =$

$$\left[Mg^{2+}\right]_{bound,i} = \frac{\left(K_{Ai}\left[Mg^{2+}\right]_{tot} + K_{Ai}\left[RNA\right]_{tot} + 1\right)}{2K_{Ai}} - \frac{\sqrt{\left(-\left(K_{Ai}\left[Mg^{2+}\right]_{tot} + K_{Ai}\left[RNA\right]_{tot} + 1\right)\right)^2 - 4K_{Ai}{}^2\left[Mg^{2+}\right]_{tot}\left[RNA\right]_{tot}}}{2K_{Ai}} \qquad (4)$$

The amount of Mg^{2+} available for binding at a site i is thus given by the amount of Mg^{2+} that was titrated to the solution, $[Mg^{2+}]_{tot}$, minus the amount of Mg^{2+} coordinated to all the other binding sites j (*equation 5*):

$$\left[Mg^{2+}\right]_{avail,i} = \left[Mg^{2+}\right]_{tot} - \sum_{j \neq i}\left[RNA_j{\bullet}Mg^{2+}\right]_j \qquad (5)$$

$[Mg^{2+}]_{avail,i}$ is then used to re-plot the chemical shift changes of the proton resonances. Fitting these curves again to a 1:1 binding isotherm yields a new estimate of the affinity constant log $K_{A,est2}$ based on the chemical shift changes of each evaluated proton in the construct (Fig. 3). log $K_{A,est2}$ values can then be averaged in the same manner as before.

Figure 3 close to here

The procedure outlined above is iterated, with the log K_A values rising as less Mg^{2+} is available for each site in later rounds, until the change in log $K_{A,av}$ converges within the error limits. In D6-27, this was the case after five iterations (Fig. 4 and Table 1A) with the exception of the strongest binding site, the 5'-terminal triphosphate group [20]. The validity of this

procedure is supported by the fact that the non-linear least square curve fits represent the experimental data much better than before (Fig. 3).

Figure 4 close to here

To obtain the affinity constant log $K_{A,final}$ after infinite iterations, the average log $K_{A,av}$ values of each round are plotted against the number of iterations and fit to an asymptotic function (Fig. 4). Usually after five iterations, the asymptotic fit levels off yielding the final intrinsic constants for each binding site. For D6-27 this procedure gave rise to a total increase in log K_A values of up to 0.4 log units for the internal binding sites and about 1 log unit for the terminal 5'-triphosphate group [20] (Table 1A). If the affinity constants of two binding sites are very similar, their order might change during the iterative procedure, however their error limits usually still overlap (Fig. 4 and Table 1). Generally, the largest effect of this procedure is exhibited at the strongest binding site.

4.2.3. ISTAR – A tool for calculating the Intrinsic STAbilities of RNA complexes

The above described iteration procedure is obviously highly time-consuming: At every step the available Mg^{2+} for each site at all 10 – 12 titration points needs to be calculated. With this information, non-linear least square fits for 40 – 50 protons need to be analyzed to derive the corresponding log K_A values. Furthermore, the handling of these many numbers invariably renders the whole process very error prone. We therefore automated the iteration procedure using the Matlab Toolbox (Matlab R2006a, Matworks Inc.). The respective calculation tool ISTAR is available from the authors.

The input consists of chemical shift values from NMR experiments for as many protons as possible of a titration series with the metal ion of choice. NMR titrations, especially if performed by 2D [^{1}H^{1}H]-NOESY experiments, are quite sensitive to variations in the external conditions such as temperature fluctuations and vibrations within the building. It is thus recommended to

run a first round of fitting for all protons and after careful evaluation of the fits mask outliers to avoid a bias of the data due to experimental errors. The log $K_{A,av1}$ values after the first round also give an indication on the appropriateness of the binding sites that were primarily defined by chemical shift and line-broadening data. At this point one can create an input file for each binding site and run ISTAR for as many iterations as needed. A specific function allows to stop the iteration when the change in $K_{A,av}$ becomes smaller than an initially defined tolerance. All data and plots from a single round are stored into consecutively numbered folders. With ISTAR we were able to diminish the calculation time for the determination of intrinsic stability constants of one metal ion species to a defined RNA from one week to around 100 seconds (Fig. 5).

Figure 5 close to here

4.2.4. Determination of the binding stoichiometry by ISTAR

The grouping of protons to the individual binding pockets is crucial because the number of defined coordination sites has a direct influence on the outcome of the calculation. We hypothesized that ISTAR is also of help in defining the correct number of binding pockets. To test this, we calculated log $K_{A,final}$ values for D6-27 with three and four instead of five binding sites.

Originally, the binding of two metal ions to the tetraloop region of D6-27, one at G10-C17 and U11-A16, and a second one at the tetraloop itself, including G12, U13, A14 and A15 was assumed (Figs. 2B and 4A). The simultaneous binding of two metal ions to a tetraloop has been a matter of debate: Although similar K_A values had been obtained across the whole tetraloop region spanning an area of about 14 Å across, this region appears to be too large to account for only one metal ion [30]. This interpretation is strengthened by results from fluorescence studies of metal ion binding to an RNA tetraloop [65] as well as the fact that a purine can bind two metal ions in astonishingly close distance without disturbing each other's affinity [66]. Nevertheless, it is also feasible that one single loosely bound metal ion rolls over the whole area as suggested

based on docking studies of a tetraloop into its receptor [67]. We now wanted to see whether ISTAR could strengthen one of these two cases. In a first test, we combined the log K_A values for all protons of this region into one binding site (fTL). This led to a decrease in log $K_{A,final}$ of each averaged site by 0.08-0.2 log units, with the exception of the terminal 5'-triphosphate, which decreased by 0.57 log units (–73%, Table 1B, Fig. 4B). The log $K_{A,final,fTL}$ of the combined tetraloop binding site, now containing proton chemical shifts from G10, U11, G12, U12, A14, A15 and C17, is 2.06 ± 0.03. This value is 0.19 log units (–35%) smaller than log $K_{A,final,H2}$ = 2.25 ± 0.03 and 0.08 log units (–17%) smaller than $K_{A,final,TL}$ 2.14 = ± 0.03 (Table 1A,B).

To confirm the trend of a decrease in log K_A with less binding sites, we calculated $K_{A,final}$ values for the hypothetical case of only three binding sites within D6-27. To do so, we integrated all the proton chemical shifts for the binding site Helix 1 (H1) into the pool of free protons. In this case, we reach a log $K_{A,final,BR}$ = 2.08 ± 0.03 (–50%), log $K_{A,final,fTL}$ = 1.97 ± 0.03 (–48% / –32%), log $K_{A,final,DP}$ = 2.52 ± 0.03 (–51%) and log $K_{A,final,TP}$ = 3.32 ± 0.10 (–81%). Hence, again all remaining binding sites "lose" affinity for Mg^{2+} confirming this general trend (Table 1C, Fig. 4C). Generally, this trend is logical, as by decreasing the number of binding sites, automatically the pool of unbound, i.e. free, Mg^{2+}, is increased, and hence the percentage of occupied binding sites decreases at each step of the titration.

It turns out that the asymptotic fit of the log K_A values *versus* the iteration round is best for the model with only four Mg^{2+} coordination sites in D6-27. This can be well seen at the example of the development of the log $K_{A,BR}$ values over the course of the iterative procedure (Fig. 6A). Both, the fits with five as well as with three binding sites are clearly not as good as the one of four binding sites. This can also be seen from the fit of the original experimental chemical shift data in the fifth iteration round, as is exemplified with G8H8 of D6-27 in Fig. 6B. Even though it seemed most plausible at first sight that two metal ions account for the chemical shift changes in the tetraloop region, it appears that only one single Mg^{2+} ion rolls over the top of the hairpin, covering a region of about 14 Å in diameter.

Obviously the correct definition of the number of binding sites within a RNA is essential to the calculation of affinity constants for metal binding. This is best achieved by taking into account as much information as possible, including a detailed evaluation of line-broadening studies with Mg^{2+} as well as Mn^{2+} and a careful analysis of the first fits for each proton as described above. With ISTAR it is possible to rapidly calculate affinity constants for several models with different numbers of binding pockets and choose the one that best fits the data, thereby validating the stoichiometry of a given interaction.

5. Conclusions and outlook

Metal ion coordination to RNAs is of utmost importance for the function of these biomoacromolecules [1-4]. The vast majority of metal ions are weakly bound in an "ion cloud" around the negatively charged phosphate sugar backbone compensation the overall negative charge of the RNA [68,69]. Some metal ions are coordinated more specifically in order to directly take part in the catalytic steps of ribozymes or to stabilize local structures with, e.g. accumulated negative charges. These specifically bound ions account for roughly 10% of electrostatic charge compensation can be localized in high resolution crystal structures as well as by chemical shift mapping in NMR experiments [13,50]. Theire log K_A values are mostly around 2-3, i.e. dissociation constants K_D are in the low millimolar range, which makes their characterization rather challenging [10,70].

Here we present a fast and optimized iterative procedure to calculate affinity constants log $K_{A,final}$ more accurately for the binding of metal ions to a number of specific sites within a larger RNA molecule. The raw data input in our case were chemical shift changes upon metal ion titration as input. For the RNA hairpin D6-27 with 4-5 Mg^{2+} coordination sites, three to four iteration rounds are sufficient for the log K_A values of the internal binding sites to converge within the error limits (Table 1). Exceptions are strong binding sites like the 5'-terminal triphosphate group, which converges only later. When we plot the chemical shift of a proton as a

function of the actual Mg^{2+} concentration, after five iteration rounds the fit to the data is much better than using the Mg^{2+} concentration titrated at each step. Hence, by taking the Mg^{2+} concentration that is bound to other binding sites into account, more accurate values for the intrinsic affinity constants log K_A of various binding sites are obtained. Due to the increased curvature of each fit in successive iteration rounds, the average log K_A values rise on average 0.4 log units after 5 iteration rounds. By fitting the plot of the log K_A of every iteration round versus the iteration round number to an asymptotic curve it is possible to estimate a log $K_{A,final}$ for full saturation of each binding site. On the other hand, ISTAR can be run easily for more iterations until all log K_A values have converged at literally no cost of time. The final log $K_{A,fin}$ values obtained by either an asymptotic fit or such an extended iteration differ in our experience at most by 0.03 log units, meaning that both procedures are valid.

This method is very sensitive to the number of defined binding sites, which has to be estimated as precisely as possible preceding the first round of calculation. Initial K_A values from conventional fitting procedures, as well as line-broadening data with Mg^{2+} and Mn^{2+} are well suited for this purpose.

An interesting problem is presented by the tetraloop of D6-27, where a large area of 13-14 Å in diameter is similarly affected by metal ion binding. Either two individual metal ions can be placed in close proximity, or one single metal ion is considered to be rolling over the whole region. Both models have been put forward in the literature [55,65,67,71-73]. We have now modeled both options by calculating the intrinsic affinity constants with the assumptions of four or five metal ion binding sites in D6-27 using ISTAR. Initially a model with five binding sites was favored [20], but the experimental data are slightly better represented by fits assuming only four sites (Fig. 6). Consequently the reevaluation of the experimental data [20] with ISTAR, now allowing a more detailed interpretation, reveals that at least in the case of D6-27 the tetraloop represents one giant binding site with one single metal ion covering a large region by dynamically rolling over an area of about 14 Å across.

The automated iterative calculation procedure ISTAR provides the means to decipher the intrinsic affinity constants for the simultaneous binding of several metal ions to one RNA. It eliminates errors arising from the assumption that Mg^{2+} exchange is fast enough to neglect metal ions bound to other sites in the calculation, as well as the need to remove excessive metal ions after every titration step as is done in the classical methods (see Section 3). While metal ion binding to RNA is certainly much more complicated in its full extend, than ISTAR is capable of describing it, ISTAR provides a large step forward in the detailed analysis of specific metal ion binding sites.

We want to emphasize that the usage of this iterative calculation method is by no means restricted to metal ion RNA interactions, but is generally applicable to any binding equilibria that involve several similarly tight interactions. Hence, ISTAR can be used for (at least) two purposes: (i) Firstly, intrinsic affinity constants for ligand binding to several sites within a given high molecular weight system (not restricted to RNA) can be rapidly calculated. (ii) Secondly, due to the short calculation time using ISTAR, various binding stochiometries can be tested. We hope that this tool will foster the better understanding of the intricate relationships between nucleic acids and their coordinated metal ions.

Abbreviations and definitions

BR	branch region in D6-27 as metal ion binding site
D5, D6	domains 5 and 6 of the group II intron *Sc*.ai5γ
D6-27	minimal domain 6 capable to support branching (27 nucleotides in length)
DP	5'-terminal diphosphate group in D6-27 as metal ion binding site
EPR	electron paramagnetic resonance
fTL	metal ion binding site in D6-27 comprising helix 2 and the tetraloop

glmS ribozyme	glucosamine-6-phosphate activated ribozyme
H1	helix 1 in D6-27 as metal ion binding site
H2	helix 2 in D6-27 as metal ion binding site
HSQC	heteronuclear singel quantum coherence
ISTAR	*I*ntrinsic *STA*bilities of RNA complexes
K_A	affinity constant
K_D	dissociation constant
NOESY	nuclear Overhauser effect spectroscopy
NMR	nuclear magnetic resonance
Sc.ai5γ	group II intron ribozyme from *Saccharomyces cerevisiae*
TL	tetraloop region in D6-27 as metal ion binding site
TP	5'-terminal triphosphate group in D6-27 as metal ion binding site

Acknowledgement

Financial support by the 7th European Framework Programme (Marie-Curie postdoctoral fellowship to MCE), the European Research Council (ERC Starting Grant 2010 MIRNA 259092 to RKOS), the Swiss National Science Foundation (RKOS), the Swiss State Secretariat for Education and Research within the COST Action D39 (RKOS), the Roche Research Foundation and the *Novartis Stiftung* (both to CF), as well as the University of Zurich is gratefully acknowledged.

Table 1. Affinity values log K_A of Mg^{2+} binding to D6-27. Shown are the averaged log K_A values at five (**A**), four (**B**) and three (**C**) high affinity binding sites, obtained from the change in chemical shifts of all aromatic and H1'-protons after five rounds of iterative correction of the [Mg^{2+}] concentration that is available at a certain site. At the 5'-end either di- or triphosphate groups are present (5'-end GDP and 5'-end GTP). In column 7, the final log $K_{A,fin}$ values after infinite iterations and in column 8 the difference in calculated stability $\Delta_{fin-meas}$ = log $K_{A,fin}$ – log $K_{A,av1}$ are given. Column 9 shows the factor F in increase of log K_A for each site from log $K_{A,av1}$ to log $K_{A,fin}$. The chemical shift changes were obtained from 2D [$^1H^1H$]-NOESY spectra of a 0.85 mM D6-27 RNA at pD 6.7 in 100 mM KCl [20]. The error limits given correspond to one standard deviation, the one of log $K_{A,fin}$ is the error of the asymptotic fit.

A

Binding site	log $K_{A,av1}$	log $K_{A,av2}$	log $K_{A,av3}$	log $K_{A,av4}$	log $K_{A,av5}$	log $K_{A,fin}$	$\Delta_{fin-meas}$	F
5'-end GDP (DP)	2.35 ± 0.04	2.56 ± 0.04	2.67 ± 0.04	2.74 ± 0.04	2.78 ± 0.05	2.83 ± 0.03	0.48 ± 0.05	3.0
5'-end GTP (TP)	3.15 ± 0.11	3.34 ± 0.11	3.49 ± 0.11	3.61 ± 0.11	3.70 ± 0.11	4.04 ± 0.10	0.89 ± 0.15	7.8
Helix 1 (H1)	1.91 ± 0.09	2.14 ± 0.08	2.23 ± 0.07	2.29 ± 0.07	2.31 ± 0.07	2.33 ± 0.03	0.42 ± 0.09	2.6
Branch Site (BR)	1.88 ± 0.10	2.12 ± 0.09	2.26 ± 0.08	2.33 ± 0.07	2.34 ± 0.08	2.38 ± 0.06	0.50 ± 0.12	3.2
Helix 2 (H2)	1.80 ± 0.14	2.06 ± 0.11	2.16 ± 0.11	2.21 ± 0.12	2.24 ± 0.12	2.25 ± 0.03	0.45 ± 0.14	2.8
Tetraloop (TL)	1.76 ± 0.09	2.00 ± 0.08	2.07 ± 0.08	2.11 ± 0.08	2.14 ± 0.08	2.14 ± 0.03	0.38 ± 0.09	2.4

B

Binding site	log $K_{A,av1}$	log $K_{A,av2}$	log $K_{A,av3}$	log $K_{A,av4}$	log $K_{A,av5}$	log $K_{A,fin}$ [a]	$\Delta_{fin-meas}$ [b]	F
5'-end GDP (DP)	2.35 ± 0.04	2.52 ± 0.04	2.59 ± 0.04	2.62 ± 0.04	2.62 ± 0.04	2.63 ± 0.03	0.28 ± 0.05	1.9
5'-end GTP (TP)	3.15 ± 0.11	3.31 ± 0.11	3.40 ± 0.11	3.43 ± 0.11	3.45 ± 0.11	3.47 ± 0.10	0.32 ± 0.15	2.1
Helix 1 (H1)	1.91 ± 0.09	2.10 ± 0.08	2.16 ± 0.07	2.18 ± 0.07	2.19 ± 0.07	2.19 ± 0.03	0.28 ± 0.09	1.9
Branch Site (BR)	1.88 ± 0.10	2.08 ± 0.09	2.16 ± 0.09	2.19 ± 0.08	2.20 ± 0.08	2.21 ± 0.03	0.33 ± 0.10	2.1
full tetraloop (fTL)	1.77 ± 0.07	1.98 ± 0.07	2.04 ± 0.07	2.05 ± 0.07	2.06 ± 0.07	2.06 ± 0.03	0.29 ± 0.08	1.9

C

Binding site	log $K_{A,av1}$	log $K_{A,av2}$	log $K_{A,av3}$	log $K_{A,av4}$	log $K_{A,av5}$	log $K_{A,fin}$ [a]	$\Delta_{fin-meas}$ [b]	F
5'-end GDP (DP)	2.35 ± 0.04	2.48 ± 0.04	2.51 ± 0.04	2.52 ± 0.04	2.52 ± 0.04	2.52 ± 0.03	0.17 ± 0.05	1.5
5'-end GTP (TP)	3.15 ± 0.11	3.27 ± 0.11	3.32± 0.11	3.32 ± 0.11	3.32 ± 0.11	3.32 ± 0.10	0.17 ± 0.15	1.5
Branch Site (BR)	1.88 ± 0.10	2.04 ± 0.10	2.07 ± 0.09	2.07 ± 0.09	2.07 ± 0.09	2.08 ± 0.03	0.19 ± 0.10	1.5
full tetraloop (fTL)	1.77 ± 0.07	1.94 ± 0.06	1.97 ± 0.07	1.97 ± 0.07	1.97 ± 0.07	1.97 ± 0.03	0.20 ± 0.08	1.5

Figure Captions

Fig. 1. Metal ion binding sites in RNA. The four natural nucleobases in RNA are shown together with their numbering scheme and the attached phosphor-sugar backbone indicated in the case of guanine. The major metal ion binding sites are shown in bold blue. Further binding sites are adenine N1 and cytosine N3, which are mostly blocked by hydrogen bonds in Watson-Crick base pairs, as well as adenine N3 [6], the ribose 2'-OH [74], as well as the bridging oxygen atoms of the phosphodiester linkage.

Fig. 2. NMR and secondary structures of two group II intron domains derived from the yeast mitochondrial intron *Sc*.ai5γ. **A** The NMR structure of the catalytic center D5 [29] with the secondary structure and the proposed metal ion binding sites [29,31] shaded in grey given below. The catalytic AGC triad is colored in green, the bulge nucleotides in gold and the tetraloop in violet. G26, which adopts a rare syn conformation and is therefore flipped down on top of the catalytic triad, is highlighted in red. **B** D6-27 structure [30] with five putative Mg^{2+} ions (golden spheres). The two top spheres probably represent two binding modes of the same Mg^{2+}. Helix 1 (nucleotides G1-G6, C22-C27) is colored in blue and helix 2 and the tetraloop (nucleotides G9-C18) in green, the branch A20 in red, and the two flanking GU wobble pairs in gold. The secondary structure of D6 with the proposed metal ion binding sites [20] shaded in grey is given below. The structures have been prepared with MOLMOL [75] based on the PDB IDs 1R2P [29] and 2AHT [30].

Fig. 3. Plot of the chemical shift change of A20 H1' of D6-27 upon addition of Mg^{2+} together with the fit of a 1:1 bimolecular association curve. The change in chemical shift (Δppm) are plotted *versus* the total Mg^{2+} concentration $[Mg^{2+}]_{tot}$ in black, as well as *versus* the actually available one as calculated in each of the five iteration rounds in grey. The final fit is indicated in red. This figure is modified from ref. [14].

Fig. 4. The average log $K_{A,av}$ values of each binding site after each iteration round are plotted *versus* the iteration number and fitted to an asymptotic function: Shown are the curves for the binding sites at the diphosphate group at the 5'-end (DP, o), in helix 1 (H1, ■), at the branch region (BR, □), beneath the tetraloop in helix 2 (H2, ▲), as well as in the tetraloop itself (TL with 5 binding sites and fTL with 4 and 3 binding sites, Δ). The curves for the binding site at the 5'-triphosphate is omitted in this figure. **A** shows the curves for the assumption that five binding sites are present in D6-27, whereas **B** shows the plots for four binding sites and **C** for three binding sites. Panel **A** is modified from ref. [20].

Fig. 5. Screenshot from a run of ISTARv2.2 needing 106.11 seconds to calculate the intrinsic affinity constants for all five Mg^{2+} binding sites in D6-27. If needed, the plots of every proton can be displayed on the screen, as exemplified here with a plot of A17 H8, but this prolongs the calculation time significantly. It is thus recommended to turn off the visualization function for the graphs while the calculation is running. They are automatically stored in a separate folder together with the least square fit, the individual K_A and log K_A values, the total free and bound fraction including their respective errors for each proton, as well as the arithmetic and weighted mean values for K_A and log K_A including errors and the fraction of bound metal ion at each titration point for every binding site. All these data can thus be reviewed at leisure after completion of the calculation.

Fig. 6. Improved non-linear least squares fit over several rounds of iteration. **A** Development of the log K_A values for the branch region over five iteration rounds when taking five (○), four (Δ), or three (□) binding sites within D6-27 into account. It can be clearly seen that the asymptotic fit is best in the case of four binding sites. **B** Fit of the experimental data for the bulge proton G8H8 opposite the branch adenosine in D6-27 in the 5th iteration round, taking five (blue, left panel),

four (red, middle panel), and three (green, right panel) binding sites within D6-27 into account. Upon close inspection it can be seen that the fit is best with four binding sites.

References

[1] A.M. Pyle, Science 261 (1993) 709-714.

[2] M.J. Fedor, Curr. Op. Struct. Biol. 12 (2002) 289-295.

[3] R.K.O. Sigel, Eur. J. Inorg. Chem. 12 (2005) 2281-2292.

[4] R.K.O. Sigel, A.M. Pyle, Chem. Rev. 107 (2007) 97-113.

[5] G.J. Narlikar, D. Herschlag, Annu. Rev. Biochem. 66 (1997) 19-59.

[6] L. Kapinos, B.P. Operschall, E. Larsen, H. Sigel, Chem. Eur. J. 17 (2011) in press.

[7] R.B. Martin, Met. Ions Biol. Syst. 32 (1996) 61-89.

[8] R.K.O. Sigel, H. Sigel, Acc. Chem. Res. 43 (2010) 974-984.

[9] R.K.O. Sigel, H. Sigel, Met. Ions Life Sci. 2 (2007) 109-180.

[10] E. Freisinger, R.K.O. Sigel, Coord. Chem. Rev. 251 (2007) 1834-1851.

[11] S.C. Dahm, O.C. Uhlenbeck, Biochemistry 30 (1991) 9464-9469.

[12] M. Roychowdhury-Saha, D.H. Burke, RNA 12 (2006) 1846-1852.

[13] J. Schnabl, R.K.O. Sigel, Curr. Op. Chem. Biol. 14 (2010) 269-275.

[14] M.C. Erat, R.K.O. Sigel, Met. Ions Life Sci. 9 (2011) 37-100.

[15] K. Klawuhn, J.A. Jansen, J. Souchek, G.A. Soukup, J.K. Soukup, ChemBioChem 11 (2010) 2567-2571.

[16] V.J. DeRose, Curr. Op. Struct. Biol. 13 (2003) 317-324.

[17] S. Nakano, A.L. Cerrone, P.C. Bevilacqua, Biochemistry 42 (2003) 2982-2994.

[18] X.W. Fang, P. Thiyagarajan, T.R. Sosnick, T. Pan, Proc. Natl. Acad. Sci. USA 99 (2002) 8518-8523.

[19] A.M. Pyle, O. Fedorova, C. Waldsich, Trends Biochem. Sci. 32 (2007) 138-145.

[20] M.C. Erat, R.K.O. Sigel, Inorg. Chem. 46 (2007) 11224-11234.

[21] K. Lehmann, U. Schmidt, Critical Rev. Biochem. Mol. Biol. 38 (2003) 249-303.

[22] O. Fedorova, N. Zingler, Biol. Chem. 388 (2007) 665-678.

[23] D. Kruschel, R.K.O. Sigel, J. Inorg. Biochem. 102 (2008) 2147-2154.

[24] O. Fedorova, C. Waldsich, A.M. Pyle, J. Mol. Biol. 366 (2007) 1099-1114.

[25] M. Steiner, K.S. Karunatilaka, R.K.O. Sigel, D. Rueda, Proc. Natl. Acad. Sci. USA 105 (2008) 13853-13858.

[26] K.S. Karunatilaka, A. Solem, A.M. Pyle, D. Rueda, Nature 467 (2010) 935-939.

[27] M.C. Erat, R.K.O. Sigel, J. Biol. Inorg. Chem. 13 (2008) 1025-1036.

[28] M. Steiner, D. Rueda, R.K.O. Sigel, Angew. Chem. Int Ed. 48 (2009) 9739-9742.

[29] R.K.O. Sigel, D.G. Sashital, D.L. Abramovitz, A.G. Palmer III, S.E. Butcher, A.M. Pyle, Nature Struct. Mol. Biol. 11 (2004) 187-192.

[30] M.C. Erat, O. Zerbe, T. Fox, R.K.O. Sigel, ChemBioChem 8 (2007) 306-314.

[31] R.K.O. Sigel, A. Vaidya, A.M. Pyle, Nature Struct. Biol. 7 (2000) 1111-1116.

[32] M.C. Erat, H. Kovacs, R.K.O. Sigel, J. Inorg. Biochem. 104 (2010) 611-613.

[33] T.A. Steitz, J.A. Steitz, Proc. Natl. Acad. Sci. USA 90 (1993) 6498-6502.

[34] E.J. Sontheimer, P.M. Gordon, J.A. Piccirilli, Genes Dev. 13 (1999) 1729-1741.

[35] N. Toor, K.S. Keating, S.D. Taylor, A.M. Pyle, Science 320 (2008) 77-82.

[36] N. Toor, K. Rajashankar, K.S. Keating, A.M. Pyle, Nature Struct. Mol. Biol. 15 (2008) 1221-1222.

[37] R.S. Brown, B.A. Hingerty, J.C. Dewan, A. Klug, Nature 303 (1983) 543-546.

[38] R.S. Brown, J.C. Dewan, A. Klug, Biochemistry 24 (1985) 4785-4801.

[39] T. Pan, O.C. Uhlenbeck, Biochemistry 31 (1992) 3887-3895.

[40] T. Pan, B. Dichtl, O.C. Uhlenbeck, Biochemistry 33 (1994) 9561-9565.

[41] L.A. Kirsebom, J. Ciesiolka, in: R.K. Hartmann, A. Bindereif, A. Schön, E. Westhof (Eds.), Handbook of RNA Biochemistry Vol. 1, pp. 214 - 227, Wiley-VCH, Weinheim, 2008.

[42] J. Ciesiolka, D. Michalowski, J. Wrzesinski, J. Krajewski, W.J. Krzyzosiak, J. Mol. Biol. 275 (1998) 211-220.

[43] M. Dutkiewicz, J. Ciesiolka, Nucleic Acids Res. 33 (2005) 693-703.

[44] N. Polacek, S. Patzke, K.H. Nierhaus, A. Barta, Mol. Cell 6 (2000) 159-171.

[45] R.K.O. Sigel, A.M. Pyle, Met. Ions. Biol. Syst. 40 (2003) 477-512.

[46] N.G. Walter, N. Yang, J.M. Burke, J. Mol. Biol. 298 (2000) 539-555.

[47] R.A. Tinsley, N.G. Walter, Biol. Chem. 388 (2007) 705-715.

[48] S. Dorner, A. Barta, Biol. Chem. 380 (1999) 243-251.

[49] A.J. Andrews, C. Fierke, in: R.K. Hartmann, A. Bindereif, A. Schön, E. Westhof (Eds.), Handbook of RNA Biochemistry Vol. 1, pp. 251 - 258, Wiley-VCH, Weinheim, 2008.

[50] D.J. Klein, P.B. Moore, T.A. Steitz, RNA 10 (2004) 1366-1379.

[51] V. Tereshko, C.J. Wilds, G. Minasov, T.P. Prakash, M.A. Maier, A. Howard, Z. Wawrzak, M. Manoharan, M. Egli, Nucleic Acids Res. 29 (2001) 1208-1215.

[52] V. Tereshko, G. Minasov, M. Egli, J. Am. Chem. Soc. 121 (1999) 3590-3595.

[53] L. Hunsicker-Wang, M. Vogt, V.J. DeRose. (2009) in: (H. Daniel, ed.), Methods Enzymol., Vol. Volume 468, pp. 335-367, Academic Press.

[54] N. Kisseleva, S. Kraut, A. Jaschke, O. Schiemann, HFSP J. 1 (2007) 127-136.

[55] J.H. Davis, T.R. Foster, M. Tonelli, S.E. Butcher, RNA 13 (2007) 76-86.

[56] M.K. Hansen, J.-P. Simorre, P. Hanson, V. Mokler, L. Bellon, L. Beigelman, A. Pardi, RNA 5 (1999) 1099-1104.

[57] Y. Tanaka, C. Kojima, E.H. Morita, Y. Kasai, K. Yamasaki, A. Ono, M. Kainosho, K. Taira, J. Am. Chem. Soc. 124 (2002) 4595-4601.

[58] Y. Tanaka, K. Taira, Chem. Commun. 16 (2005) 2069-2079.

[59] S.E. Butcher, F.H.-T. Allain, J. Feigon, Biochemistry 39 (2000) 2174-2182.

[60] S. Johannsen, N. Megger, D. Bohme, R.K.O. Sigel, J. Müller, Nature Chem. 2 (2010) 229-234.

[61] R.L. Gonzalez, Jr., I. Tinoco, Jr., Methods Enzymol. 338 (2001) 421-443.

[62] I. Bertini, C. Luchinat (Eds.), NMR of Paramagnetic Molecules in Biological Systems, Benjamin/Cummings, Menlo Park, CA, 1986.

[63] M. Maderia, T.E. Horton, V.J. DeRose, Biochemistry 39 (2000) 8193-8200.

[64] M. Phelan, R.J. Banks, G. Conn, V. Ramesh, Nucleic Acids Res. 32 (2004) 4715-4724.

[65] M. Menger, F. Eckstein, D. Porschke, Biochemistry 39 (2000) 4500-4507.

[66] B. Knobloch, R.K.O. Sigel, B. Lippert, H. Sigel, Angew. Chem., Int. Ed. 43 (2004) 3793-3795.

[67] C.D. Downey, J.L. Fiore, C.D. Stoddard, J.H. Hodak, D.J. Nesbitt, A. Pardi, Biochemistry 45 (2006) 3664-3673.

[68] V.B. Chu, Y. Bai, J. Lipfert, D. Herschlag, S. Doniach, Curr. Op. Chem. Biol. 12 (2008) 619-625.

[69] D.E. Draper, D. Grilley, A.M. Soto, Annu. Rev. Biophys. Biomol. Struct. 34 (2005) 221-243.

[70] S. Johannsen, M.M.T. Korth, J. Schnabl, R.K.O. Sigel, Chimia 63 (2009) 146-152.

[71] P.Z. Qin, S.E. Butcher, J. Feigon, W.L. Hubbell, Biochemistry 40 (2001) 6929-6936.

[72] P.Z. Qin, J. Feigon, W.L. Hubbell, J. Mol. Biol. 351 (2005) 1-8.

[73] J.H. Davis, M. Tonelli, L.G. Scott, L. Jaeger, J.R. Williamson, S.E. Butcher, J. Mol. Biol. 351 (2005) 371-382.

[74] F.M. Al-Sogair, B.P. Operschall, A. Sigel, H. Sigel, J. Schnabl, R.K.O. Sigel, Chem. Rev. 111 (2011) in press, doi: 10.1021/cr100415s.

[75] R. Koradi, M. Billeter, K. Wüthrich, J. Mol. Graphics 14 (1996) 29-32 & 51-55.

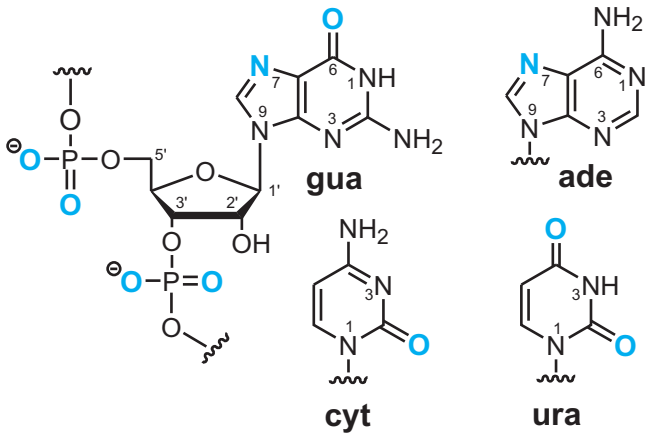

Figure 1

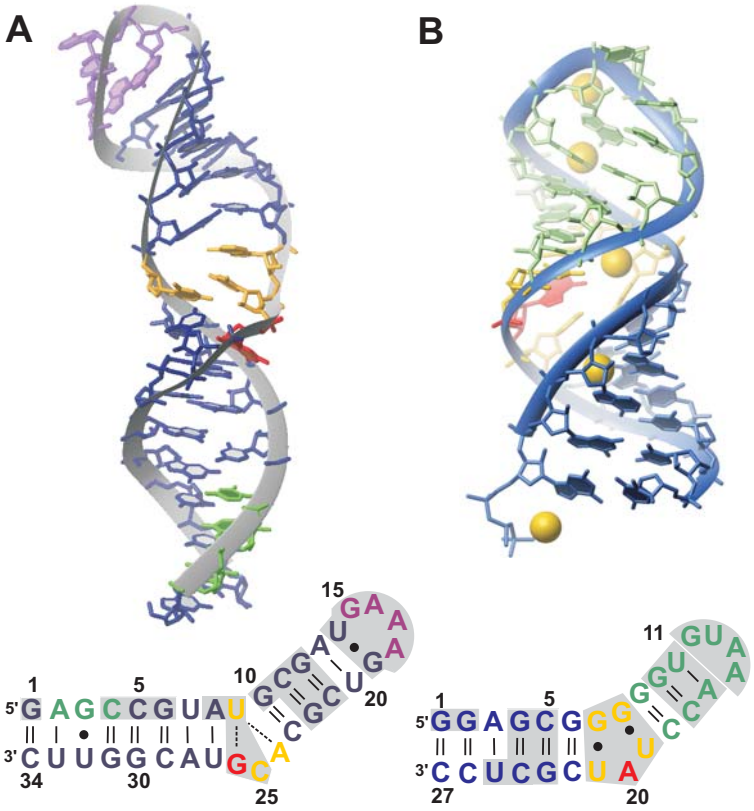
A
B
1
5
10
15
20
25
30
34
5'G A G C C G U A U
3'C U U G G C A U G C
G A A
U
A
G
G C
C G
G C
U
A
C
11
GU A
A
G
U
G
C
A
G
C
5'G G A G C G G
3'C C U C G C U A U
1
5
11
20
27

Figure 2

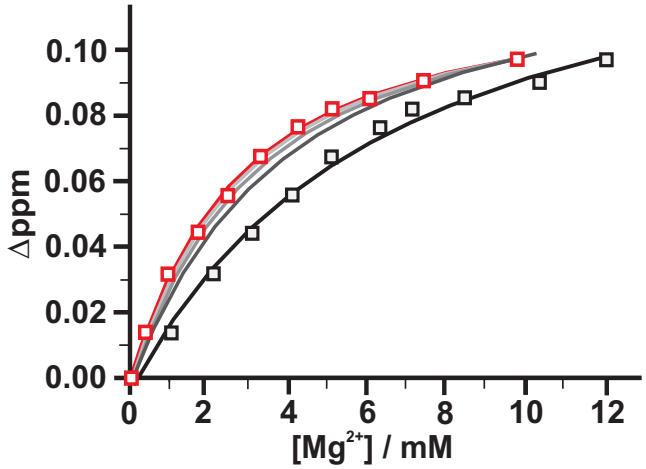

Figure 3

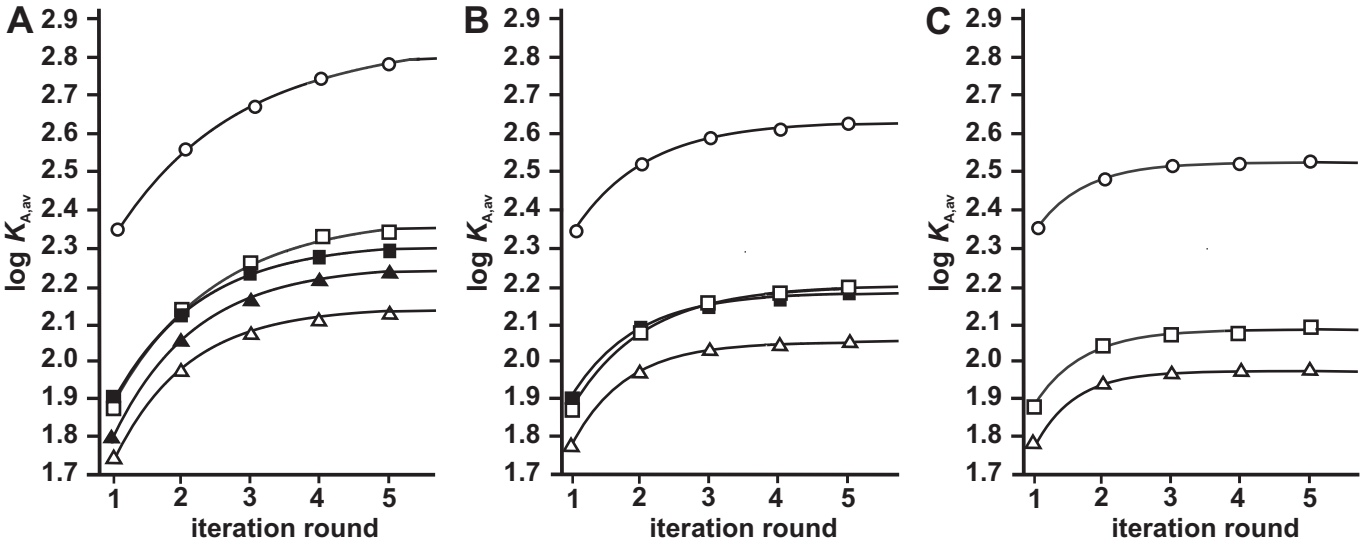
A
B
C
log $K_{A,av}$
2.9
2.8
2.7
2.6
2.5
2.4
2.3
2.2
2.1
2.0
1.9
1.8
1.7
1
2
3
4
5
iteration round

Figure 4

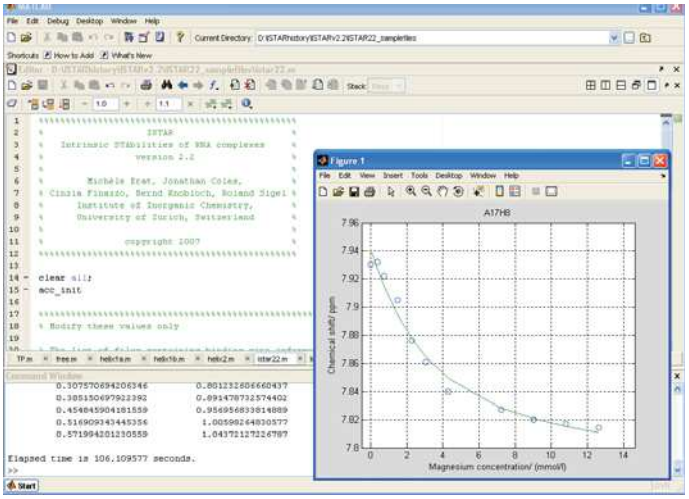
ISTAR
Intrinsic STAbilities of RNA complexes
version 2.2
Michèle Brat, Jonathan Coles,
Cinzia Finazzo, Bernd Knobloch, Roland Sigel
Institute of Inorganic Chemistry,
University of Zurich, Switzerland
copyright 2007
clear all;
acc_init
% Modify these values only
Elapsed time is 106.109577 seconds.
Figure 1
A17HB
Chemical shift/ ppm
Magnesium concentration/ (mmol/l)

Figure 5

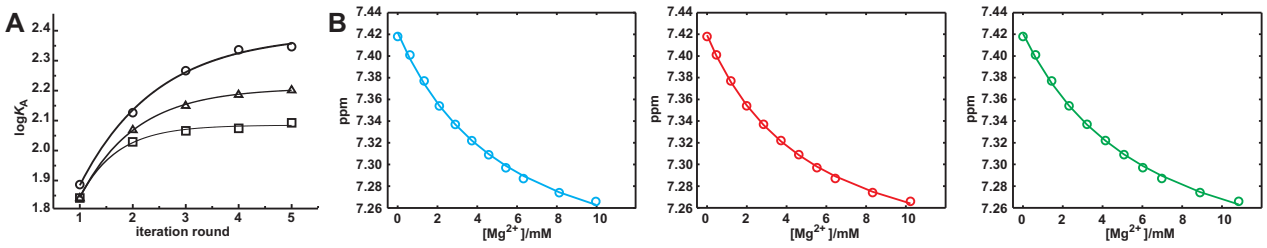

Figure 6